

Spatiotemporally Distinct Protein Kinase D Activation in Adult Cardiomyocytes in Response to Phenylephrine and Endothelin^{*[S]}

Received for publication, March 31, 2011, and in revised form, July 18, 2011. Published, JBC Papers in Press, July 27, 2011, DOI 10.1074/jbc.M111.246447

Julie Bossuyt⁺¹, Chia-Wei Chang^{+§}, Kathryn Helmstadter⁺, Maya T. Kunkel[¶], Alexandra C. Newton[¶], Kenneth S. Campbell^{||}, Jody L. Martin[§], Sven Bossuyt^{**}, Seth L. Robia[§], and Donald M. Bers⁺²

From the ⁺Department of Pharmacology, University of California, Davis, California 95616, the [§]Department of Physiology, Loyola University Chicago, Maywood, Illinois 60153, the [¶]Department of Pharmacology, University of California, San Diego, California 92093, the ^{||}Department of Physiology, University of Kentucky, Lexington, Kentucky 40536, and the ^{**}Department of Engineering Design and Production, Aalto University School of Science and Technology, Helsinki, Finland FI-02015

Protein kinase D (PKD) is a nodal point in cardiac hypertrophic signaling. It triggers nuclear export of class II histone deacetylase (HDAC) and regulates transcription. Although this pathway is thought to be critical in cardiac hypertrophy and heart failure, little is known about spatiotemporal aspects of PKD activation at the myocyte level. Here, we demonstrate that in adult cardiomyocytes two important neurohumoral stimuli that induce hypertrophy, endothelin-1 (ET1) and phenylephrine (PE), trigger comparable global PKD activation and HDAC5 nuclear export, but via divergent spatiotemporal PKD signals. PE-induced HDAC5 export is entirely PKD-dependent, involving fleeting sarcolemmal PKD translocation (for activation) and very rapid subsequent nuclear import. In contrast, ET1 recruits and activates PKD that remains predominantly sarcolemmal. This explains why PE-induced nuclear HDAC5 export in myocytes is totally PKD-dependent, whereas ET1-induced HDAC5 export depends more prominently on InsP₃ and CaMKII signaling. Thus α -adrenergic and ET-1 receptor signaling via PKD in adult myocytes feature dramatic differences in cellular localization and translocation in mediating hypertrophic signaling. This raises new opportunities for targeted therapeutic intervention into distinct limbs of this hypertrophic signaling pathway.

Various stresses trigger cardiac hypertrophy, remodeling, and functional alterations (1, 2). Prolonged stress can also become maladaptive, leading to heart failure, cardiac arrhythmias, and sudden death. Many of these changes are mediated by altered gene expression, and Class II histone deacetylases (HDACs)³ (e.g. HDAC5) are recognized as key modulators of

this genetic reprogramming. HDAC5 represses transcription by promoting more condensed DNA, and represses transcription factors such as myocyte enhancing factor 2 (MEF2). HDAC5 phosphorylation triggers its nuclear export (allowing gene activation (Fig. 1a)). Both protein kinase D (PKD) and calmodulin-dependent protein kinase II (CaMKII) are key HDAC kinases (1, 2) and accumulating evidence indicates both kinases are more active in heart failure and can contribute directly to cardiac pathogenesis (3–6).

Cardiac PKD is activated in response to hypertension, pressure overload, and chronic neurohumoral signaling (7). Overexpression of constitutively active PKD (and CaMKII δ) cause cardiac hypertrophy followed by chamber dilation (8, 9). Moreover there is increased expression of PKD (and CaMKII δ) in failing rat, rabbit, and human myocardium (8, 10). Thus, whereas PKD and CaMKII activation may be involved in a wide variety of cell functions (11–14), they are attractive potential therapeutic targets in cardiac disease. Therapeutic benefit of PKD/CaMKII inhibition may be largely due to prevention of HDAC (class II) phosphorylation, thereby maintaining the repressive effects of HDAC on transcription. Indeed, HDAC5 knock-out mice develop profound pathological cardiac hypertrophy and HDAC5 overexpression can limit progression of cardiac hypertrophy (15, 16). On the other hand, HDAC inhibition is a promising chemotherapeutic strategy in cancer (17–21). HDAC subtype-specific inhibition might be a way to resolve this benefit conflict, but targeting upstream of HDACs may hold unique benefits. Along these lines, cardiac-specific deletion of PKD1 (and CaMKII δ knock-out) limit cardiac remodeling after aortic constriction (5, 22) and novel PKD inhibitors have had some success in the prevention of pathological hypertrophy (23–25) as well as of pancreatic and prostatic cancer growth (17, 26). In the heart, a better mechanistic understanding of how cardiomyocyte PKD and CaMK are activated in response to pathogenic neurohumoral stimuli (5–6) is needed to evaluate the therapeutic potential of specific PKD/CaMKII inhibition.

PKD (previously termed PKC μ) exhibits 3 isoforms, of which PKD1 is the predominant cardiac isoform. This serine/threo-

* This work was supported, in whole or in part, by National Institutes of Health Grants R01HL103933 (to J. B.), P01-HL80101 (to D. M. B.), P01-DK5441 (to A. C. N.), and T32HL86350 (to K. H.), American Heart Association Grant SDG 0835312N (to J. B.) and a predoctoral fellowship (to C. W. C.), and a grant from the FWO-Vlaanderen and Academy of Finland (to S. B.).

[S] The on-line version of this article (available at <http://www.jbc.org>) contains supplemental Fig. S1 and Movies S1 and S2.

¹ To whom correspondence may be addressed: Genome Building 3511, Davis, CA 95616-8636. Fax: 530-752-7710; E-mail: jbossuyt@ucdavis.edu.

² To whom correspondence may be addressed. E-mail: dmbers@ucdavis.edu.

³ The abbreviations used are: HDAC, histone deacetylase; PKD, protein kinase D; CaMK, calmodulin-dependent protein kinase; DAG, diacylglycerol; ET1, endothelin-1; PE, phenylephrine; TIRF, total internal reflection fluorescence

microscopy; SL, sarcolemma; FAP, fluorescence recovery after photobleach; InsP3R, inositol 3-trisphosphate receptor; PDBu, phorbol 12,13-dibutyrate; DKAR, D kinase activity reporter.

nine kinase consists of a C-terminal catalytic core and an N-terminal regulatory moiety with two cysteine-rich regions (C1a and C1b) and a pleckstrin homology domain (27–29). Like in PKC (30), the C1 domains of PKD impart reversible membrane recruitment in response to G protein-coupled receptor-induced production of diacylglycerol (DAG), or in response to phorbol esters. The classical pathway for PKD activation involves a membrane recruitment phase and PKC-mediated phosphorylation of serine residues within the activation loop of the catalytic domain (Ser⁷⁴⁴/Ser⁷⁴⁸), followed by autophosphorylation at serine 916 (near the C terminus) (31–35). Recent work has also raised the possibility of Ca²⁺-dependent PKD activation (36, 37). In cultured neonatal rat ventricular myocytes PKD is the predominant HDAC5 kinase (7). However, in adult ventricular myocytes PKD expression is greatly reduced (38), and we have shown that PKD contributes equally with CaMKII in governing endothelin-1 (ET1)-induced HDAC5 nuclear export (37).

We previously identified a novel and entirely InsP₃- and Ca/CaM-dependent process in ET1-induced HDAC5 nuclear export and transcriptional regulation in adult cardiomyocytes (37). The α -adrenergic receptor agonist phenylephrine (PE) can also induce HDAC5 nuclear export and is known to induce cardiac remodeling (7). Here we show that PE and ET1 (both acting via G_q-coupled receptors) induce comparable global PKD activation, HDAC5 nuclear export, and transcriptional activation in adult cardiomyocytes, but that the subcellular signaling via PKD differ dramatically. PE signaling was totally InsP₃- and Ca/CaMKII-independent, in contrast to ET1 (where InsP₃, calmodulin, and CaMKII are critical players). Moreover, PE induced very rapid and transient PKD recruitment and activation at the sarcolemma, followed by rapid PKD translocation to the nucleus. In contrast ET1 cause more stable PKD recruitment to the sarcolemma, with less nuclear translocation.

EXPERIMENTAL PROCEDURES

Myocyte Isolation and Adenoviral Infection—All animal and biohazard protocols were approved by the appropriate committees at the University of California, Davis. Rabbit ventricular myocytes were isolated as previously described (39) and plated on laminin-coated culture inserts. Culture medium was PC-1 (Cambrex) supplemented with 5% penicillin-streptomycin. Myocytes were infected for 2 h (multiplicity of infection 10–50) with recombinant replication-deficient adenovirus expressing HDAC5-GFP, PKD1-GFP, or DKAR variants, with subsequent culture for 20–30 h. GFP fluorescence (CFP/YFP for DKARs) indicated infection and localization. For non-targeted DKAR experiments, ventricular myocytes were also infected with adenovirus encoding PKD1. To ensure adequate infection of myocytes (lack of GFP expression), protein expression of PKD was assessed by Western blotting. After 24 h, myocytes were exposed for 1 h to 100 nM ET-1, 10 μ M PE, 200 nM PDBu or vehicle as indicated. These experiments were performed with or without 1 μ M KN-93, 10 μ M BisI, 2 μ M 2-APB (2-aminoethoxydiphenyl borate), or 10 μ M Gö6967 pretreatment for 20 min.

Immunoblotting and Immunocytochemistry—Isolated myocytes were rinsed in PBS and treated as indicated before lysing

in ice-cold buffer containing in mM: 150 NaCl, 10 Tris (pH 7.4), 2 EGTA, 50 NaF, 0.2 NaVO₃, 1% Triton X-100, and protease and phosphatase inhibitor mixture III (Calbiochem). Cell lysates were flash-frozen and stored at –80 °C. Proteins were size fractionated on 8% SDS-PAGE before transferring to a 0.2- μ m nitrocellulose membrane. Immunoblots were blocked with 5% milk in Tris-buffered saline, Tween. The blots were then incubated overnight at 4 °C with primary antibody: PKD, PKD-phospho-Ser⁹¹⁶, or PKD-phospho-Ser⁷⁴⁴/Ser⁷⁴⁸ (1:1000; Cell Signaling). After incubation with the HRP-labeled secondary antibody, blots were developed using enhanced chemiluminescence (Pierce SuperSignal). All signals were recorded using a UVP-EpichemII darkroom imaging system for quantification and captured on film for representation. Equal protein loading was ensured by reprobing for GAPDH (1:5000; Abcam). All experiments were performed in duplicate.

For immunostaining, myocytes seeded on glass coverslips were fixed with 4% paraformaldehyde in PBS. After incubation in PBS with 0.1% glycine, cells were permeabilized with 1% Triton X-100 and incubated with anti-PKD (1:50, overnight, 4 °C). This was visualized with anti-rabbit (Alexa 488).

Confocal Measurements—GFP-HDAC5 and PKD1-GFP signals were measured by confocal microscopy with argon laser excitation at 488 nm and emitted fluorescence (F) at LP 500. Image J software was used for analysis with the intensity of the regions of interest normalized to area. Fluorescence intensities were also corrected for background signal. For quantification of recruitment to Z-lines, a plot profile was fitted to a sinusoidal equation, and the amplitude was taken as the Z-line signal.

Fluorescence Resonance Energy Transfer (FRET) Measurements—FRET was measured 2 ways (1). A non-destructive, ratiometric technique was used to monitor time-dependent FRET changes (and this also helped to verify that the DKAR signal was not saturated under the conditions used). In this method CFP and YFP emission are measured upon CFP excitation (the relative abundance of donor and acceptor is not an issue for DKAR) (40). The following protocol was used: 100-ms acquisitions of CFP image (CFP excitation and emission), 100-ms acquisitions of YFP image (YFP excitation and emission), and finally 100-ms acquisition of FRET image (CFP excitation but YFP emission). This is then followed by the second approach, the acceptor photobleach method, where FRET efficiency was measured quantitatively as the increase in donor (CFP) fluorescence upon YFP photobleaching (which eliminates energy transfer from the donor to YFP) (40). Here, YFP was progressively photobleached using 100-ms acquisitions of the CFP image, 40-ms acquisitions of the YFP image, followed by repeated 10-s exposure to the YFP-selective photobleach (504/12 nm excitation). This protocol has been validated with FRET-standard samples (41).

Fluorescence imaging utilized an inverted microscope equipped with a 1.49 NA objective, and a back-thinned CCD camera (iXon 887, Andor Technology). Image acquisition and acceptor photobleaching was automated with custom software macros in MetaMorph that controlled motorized excitation/emission filter wheels (Sutter Instrument Co.) with filters for CFP (excitation 427/10, emission 472/30 nm) and YFP (excitation 504/12 nm, emission 542/27) (Semrock).

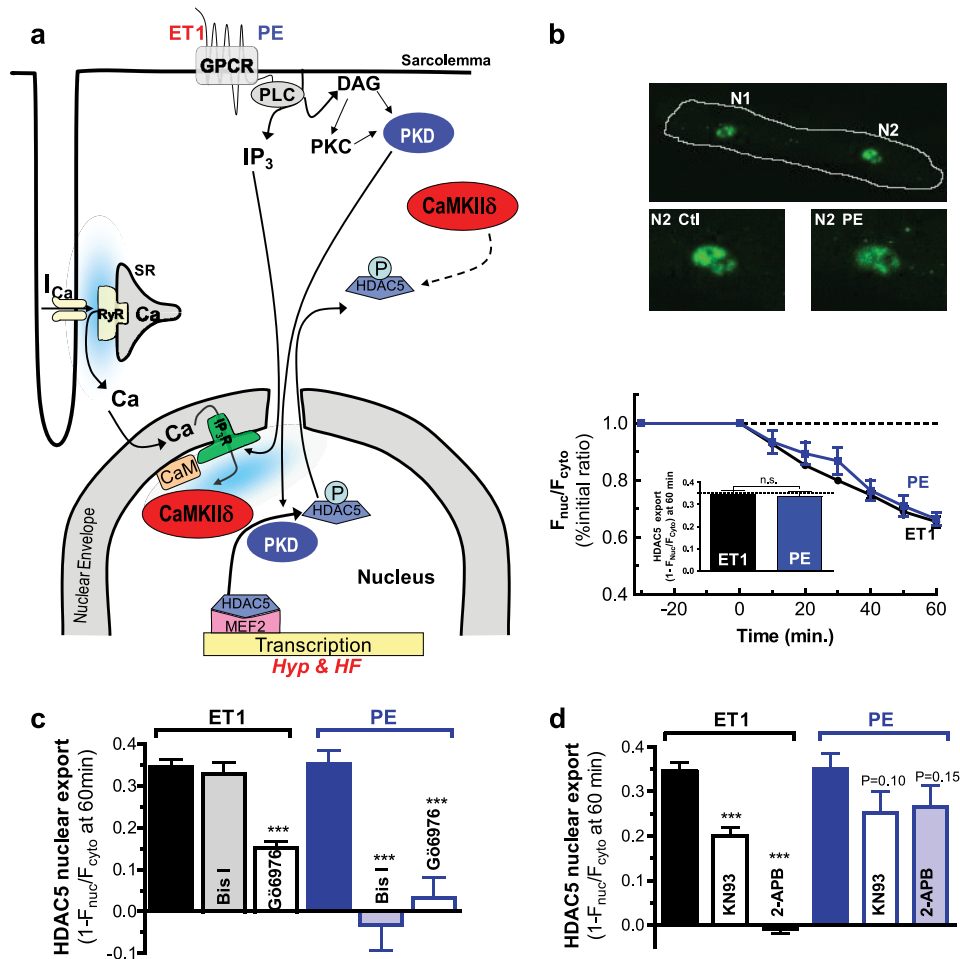


FIGURE 1. Agonist-dependent signaling to HDAC5. *a*, signaling pathway to HDAC5 nuclear export. G protein-coupled receptor (GPCR) activation leads to InsP₃ production, which in turn causes local, nuclear Ca²⁺ release and CaMKII/PKD activation. These kinases then phosphorylate HDAC5 triggering its nuclear export. *b*, rabbit ventricular myocyte expressing GFP-HDAC5 exposed to 10 μM PE, with enlargements of the nucleus (N2) region before and after a 60-min PE exposure. HDAC5 nuclear export was analyzed as a decrease of F_{nuc}/F_{cyto} normalized to the initial ratio (*n* = 12 for 100 nM ET1, 20 for 10 μM PE). *c*, myocytes were pretreated with 10 μM Bis I or Gö6976 for 20–30 min before ET1 or PE exposure for 60 min. *d*, myocytes were pretreated with 1 μM KN93 or 2 μM 2-APB for 20–30 min prior to ET1 or PE exposure (***, *p* < 0.001).

“Prismless” TIRF Measurements (Total Internal Reflection Fluorescence Microscopy)—Argon laser light (488/5 nm) was directed through the objective with a multiple band dichroic mirror. TIRF emission was selected with filters (515/30 nm for GFP). Filter transitions and shutter events were automated with acquisition software. 250-Millisecond exposure images were obtained continuously.

Spatially Resolved Photobleaching in TIRF Mode—The laser-line was selected as above and directed to the sample with a 10/90 beam splitter. Laser photobleach exposure was controlled by a Uniblitz shutter to 500 ms. Acquisition parameters were optimized to minimize photobleaching so the following images (250 ms exposure) were obtained sequentially (as in Fig. 5*a*): 9 images every 30 s, 10 consecutive images followed by a bleach pulse, 15 consecutive images, 6 images every 20 s, 10 images every 30 s. Postbleach images were normalized to an averaged prebleach image to visualize *F*/*F*₀ image time series. The spatial profile of the normalized bleach spot was characterized by bell-shaped profiles that were described by a Gaussian form (42). Analysis of the evolution of the bleach spot was performed, using a custom interface to the optimization tool-

box in Matlab, by fitting image data in a regularized least squares sense to the formula,

$$F_{(\bar{x},t)} = F_0(\bar{x}) \times \left(b_{(t)} - \frac{V_{\text{peak}}^{(t)}}{w_{\text{peak}}^2} \exp\left(-\frac{\|\bar{x} - \bar{x}_c\|^2}{w_{\text{peak}}^2}\right) \right)$$

where *b* is the base fluorescence outside the bleach region (fit independently of the bleach spot), *V*_{peak} is proportional to the integral of the bell shape, *w*_{peak} is the width of the bleach spot, and *x*_c is the position of its center.

Statistical Analysis—Data are expressed as mean ± S.E. Statistical discriminations were performed with Student’s *t* test (paired when appropriate) and analysis of variance with *p* < 0.05 was considered significant.

RESULTS

Role of PKD in the Regulation of HDAC—ET1-induced HDAC5-GFP nuclear export and excitation-transcription coupling in adult cardiac myocytes is entirely dependent on local InsP₃-induced Ca²⁺ release and CaM, and depends equally on CaMKII and PKD phosphorylation of HDAC5 (Fig. 1*a*) (37).

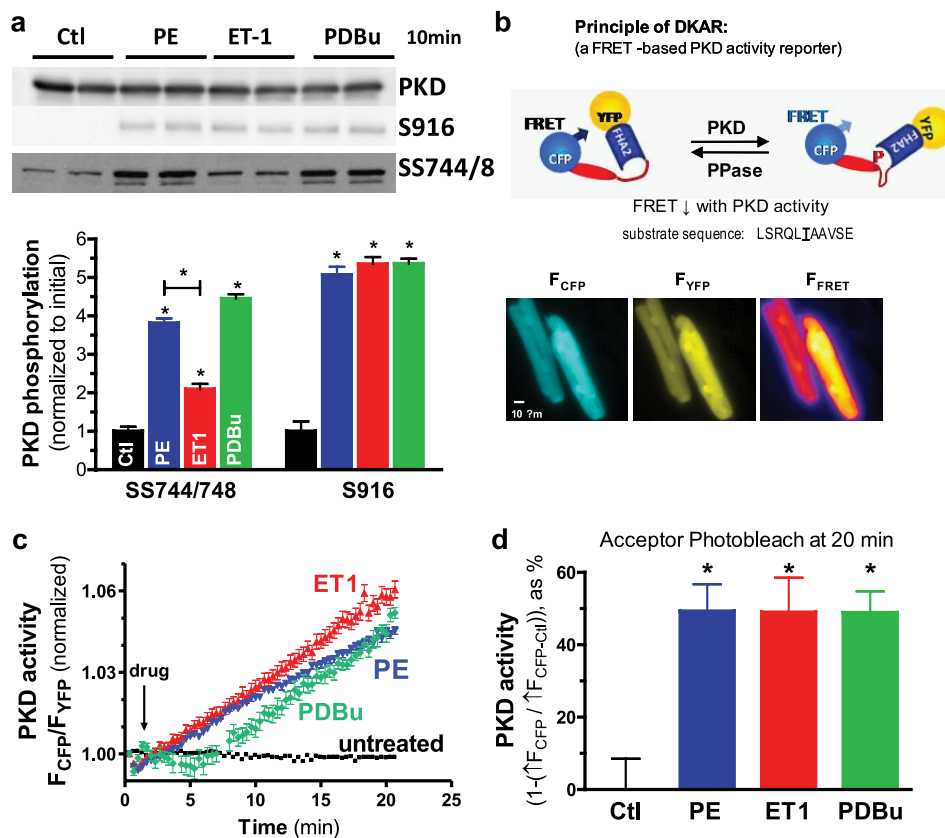


FIGURE 2. **Assessment of global PKD activation.** *a*, representative Western blots of PKD expression and phosphorylation (using global and phosphospecific antibodies) in adult rabbit myocytes and quantified protein signals ($n = 6$). *b*, principle of DKAR measurements of PKD activity (adapted from Kunkel *et al.* (25)), upon phosphorylation of the substrate sequence a molecular switch occurs resulting in a decrease of FRET. Expression of the sensor is shown in rabbit myocytes with selective excitation of CFP, YFP, or FRET (excitation of CFP, detection of YFP emission). *c*, ratiometric real time measurements of DKAR FRET in adult rabbit myocytes (also expressing PKD1, $n = 6$). *d*, acceptor photobleach-induced enhancement of CFP fluorescence (DKAR FRET) after 20 min exposure to PE, ET1, or PDBu ($n = 6$). Data are presented as the % change obtained, assuming that fully phosphorylated DKAR depicts no basal FRET.

Fig. 1*b* shows that in adult rabbit ventricular myocytes PE (another G_q -coupled receptor hypertrophic agonist) produces very similar HDAC5-GFP nuclear export to ET1 (34 ± 2 versus $35 \pm 2\%$ at 60 min). Control studies confirmed that the ET1 and PE concentrations used are maximally activating. However, PKC inhibition (with BisI) virtually abolished PE-induced HDAC5 nuclear export, without altering that induced by ET1 (Fig. 1*c*). Also PKD blockade (with Gö6976, a PKC/PKD inhibitor) caused $\sim 50\%$ inhibition of ET1-induced HDAC5 translocation, and again completely blocked the PE-induced effect. Conversely, pretreatment with the CaMKII inhibitor KN93 or the InsP_3 blocker 2-APB did not significantly alter the PE response, but potently inhibited the ET1-induced HDAC5 nuclear export (Fig. 1*d*). Parallel effects were observed for PE- versus ET1-induced myocyte enhancing factor 2 transcriptional activation, using a myocyte enhancing factor 2-luciferase reporter construct in adult rabbit ventricular myocytes (not shown). These experiments indicate that PKC-dependent PKD activation is required for PE-induced HDAC5 nuclear export (independent of InsP_3 -dependent Ca release or CaMKII). This contrasts with the ET1-dependent pathway, which requires InsP_3 -sensitive calcium stores and both CaMKII plus PKD, but not PKC. Thus, each G_q -coupled receptor agonist (ET1 and PE) activates divergent signaling pathways in adult cardiac myocytes. This also indicates that ET1-induced PKD activation

might be PKC independent, whereas that by PE requires PKC. Notably, inhibition of PLC by U73122 blocks PKD activation by both ET1 and PE, consistent with DAG-dependent activation of PKD that is independent of PKC, as suggested by previous work (8, 38).

Do PE and ET1 Differ in Their Ability to Activate PKD1?—Fig. 2*a* shows that exposure to PE, ET1, or the phorbol ester PDBu cause a similar 5-fold increase in PKD autophosphorylation levels at Ser⁹¹⁶ (often used as a read-out of PKD1 activity). PE and PDBu both strongly activated phosphorylation of the activation loop Ser⁷⁴⁴/Ser⁷⁴⁸ sites on PKD1 (by ~ 4 -fold), but ET1 was much less effective in causing phosphorylation at Ser⁷⁴⁴/Ser⁷⁴⁸. Because PKC is known to phosphorylate these sites (32, 33), this is consistent with the more pronounced PKC dependence for PE-induced HDAC5 nuclear export (versus ET1; Fig. 1*c*).

To more directly measure PKD activity and activation time course in adult cardiac myocytes, we used the FRET-based PKD activation reporter (DKAR) (36). DKAR includes a PKD-specific substrate and phosphoamino acid-binding domain linking CFP and YFP, such that upon phosphorylation by PKD, FRET is reduced (Fig. 2*b*). Monitoring the CFP/YFP ratio, we found that PE and ET1 activated global PKD activity to a similar degree in adult myocytes (Fig. 2*c*). We also used an additional DKAR FRET measurement, *i.e.* donor fluorescence enhancement

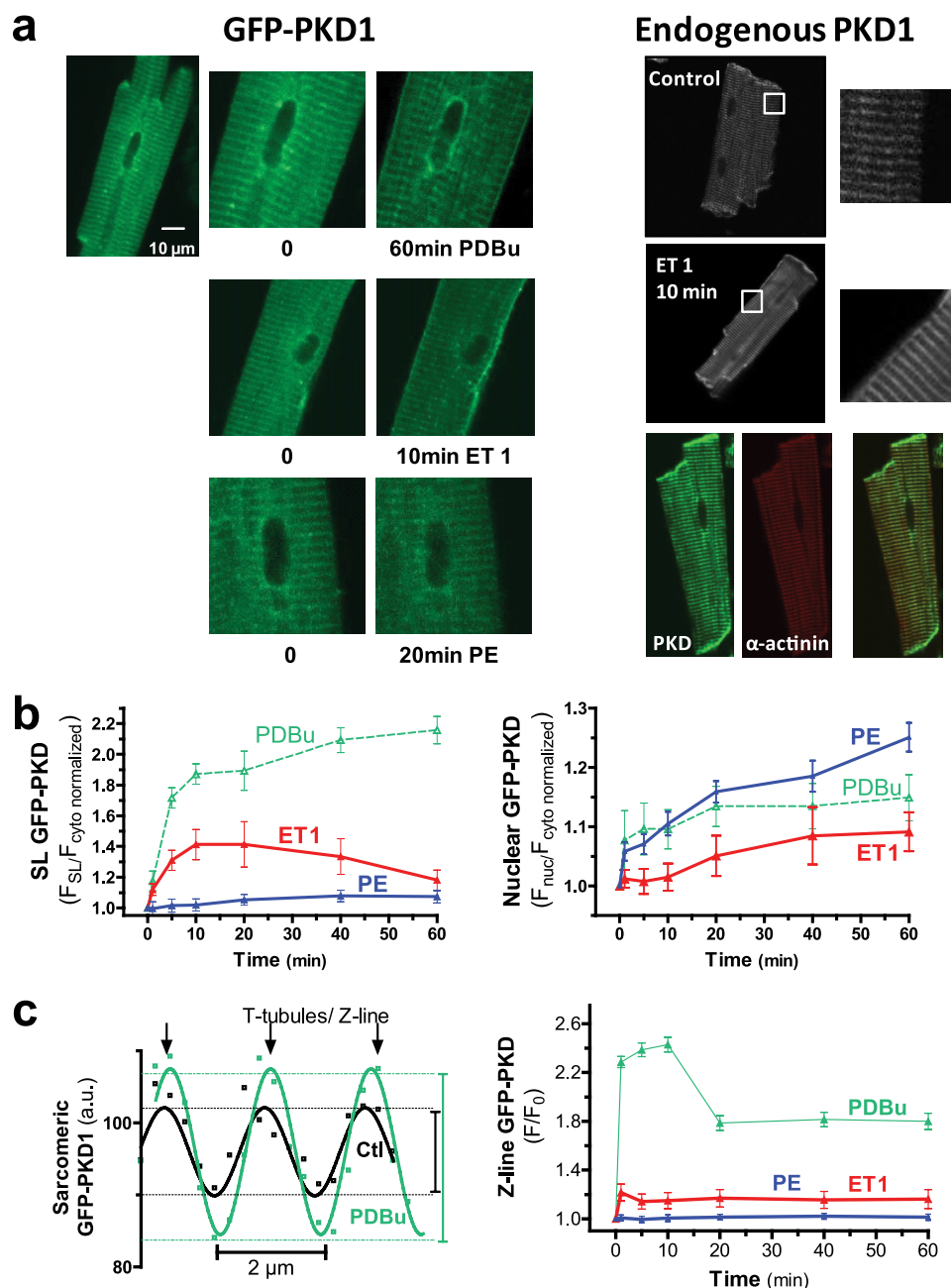


FIGURE 3. **Agonist-dependent spatiotemporal dynamics of PKD1 localization.** *a*, rabbit ventricular myocyte expressing PKD1-GFP exposed to PDBu (top left), ET1 (middle left), and PE (bottom left). Right panels show immunolocalization of endogenous PKD1 in non-transfected myocytes. Right bottom panels show (b) PKD1-GFP localization was analyzed as F_{SL}/F_{cyto} and F_{nuc}/F_{cyto} for membrane recruitment and nuclear import, respectively ($n \geq 5$; all 3 curves were significantly different (left) and ET1 was different from PE and PDBu (right) by analysis of variance). *c*, for analysis of recruitment to T-tubular membrane (or Z-line), plot profiles were fit to a sine wave (left) and amplitude was taken as Z-line signal (right, ET1 was different from PE by analysis of variance).

upon acceptor photobleach (Fig. 2*d*). This quantitative method also showed similar PKD activity after 20 min exposure to PE, ET1, and PDBu. These results are consistent with our *in vitro* surrogate measure of PKD activity (phospho-S916 PKD) in Fig. 2*a*. These changes in DKAR FRET were reversible upon agonist withdrawal and blocked by pretreatment with Gö6976 (not shown).

The similar PKD activation by PE and ET1 in Fig. 2 does not explain how these two G_q -coupled receptors differently affect HDAC5 nuclear export and transcriptional activation (*i.e.* why is PKD much more critical for PE *versus* ET1 signaling to the nucleus?). It is possible that PKD localization and translocation

differ for PE and ET1, as PKD can redistribute among intracellular targets in other cell types (43, 44). We explored this using PKD1-GFP fusion proteins expressed in adult rabbit ventricular myocytes using an adenoviral vector.

Spatiotemporal Dynamics of PKD1 Localization in Response to PE and ET1—Confocal imaging of adenovirally expressed PKD1-GFP fusion protein and immunostained endogenous PKD1 revealed that at rest, PKD1 expression is relatively uniform and cytosolic (slightly higher at Z-line/transverse tubule region), and largely non-nuclear (Fig. 3*a*) (F_{nuc}/F_{cyto} is 0.5 ± 0.03 and 0.68 ± 0.06 , respectively). Application of ET1 caused rapid, sustained PKD recruitment to the plasma membrane or

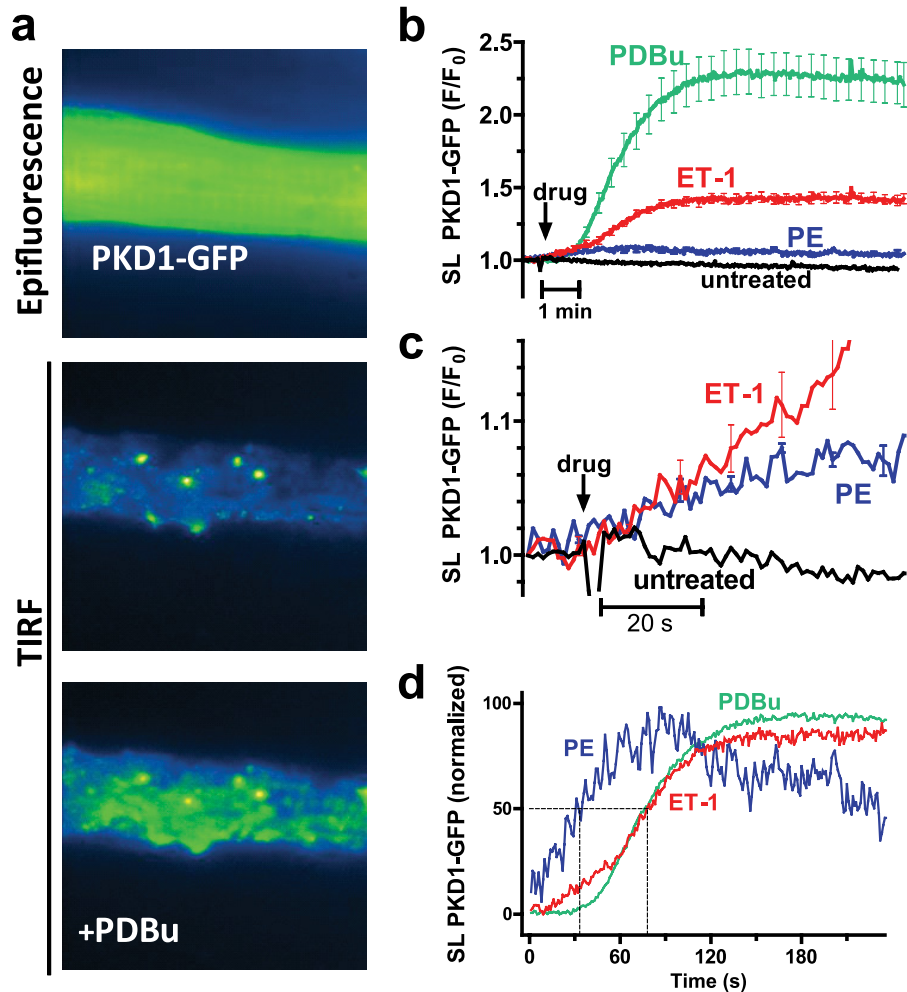


FIGURE 4. **TIRF measurements of PKD1-GFP.** *a*, rabbit ventricular myocyte expressing PKD1-GFP is shown using epifluorescence (top) and TIRF imaging (lower panels), including membrane recruitment in TIRF mode upon exposure to PDBu. *b*, agonist-dependent PKD1 membrane recruitment analyzed as increases in GFP fluorescence (normalized to initial signal) in TIRF mode ($n = 10$; all 4 curves were significantly different by analysis of variance), including the expanded display of first 75 s (*c*) and amplitude-normalized time course (*d*).

sarcolemma (SL, $39 \pm 4\%$ increase), with only a modest and much delayed nuclear import (9 ± 3 or 23% of the SL increase). In striking contrast, PE only slightly increased membrane PKD ($7 \pm 2\%$), but much more strongly increased nuclear translocation (25 ± 2 or 357% of the SL increase) (Fig. 3, *a* and *b*). Note also that the smaller rise in nuclear PKD1 concentration with ET1 happens with a clear delay and as the SL starts to decline. These findings indicate that ET1 drives SL recruitment of PKD1, whereas PE drives rapid nuclear recruitment of PKD1 (consistent with a more prominent role in nuclear HDAC5 phosphorylation). Similar results were obtained with immunostaining of endogenous PKD1 (Fig. 3*a*), validating the use of PKD1-GFP as a tracer for the endogenous protein (not all data shown). PKD1 is also recruited to the T-tubular membrane (SL invaginations in cardiac myocytes), as indicated by the sharpening of the fluorescence intensity at the Z-line/T-tubule location *versus* the mid-sarcomere region (Fig. 3*c*). Moreover, the relative strength of agonists (PDBu > ET1 > PE) causing T-tubule concentration was the same as that for surface SL (Fig. 3*b*).

To obtain more selective sarcolemmal PKD1-GFP information we used prismless TIRF microscopy. In TIRF the angled incident excitation beam is reflected by the glass coverslip on

which cells lie, such that the evanescent wave excites fluorophores only within ~ 100 nm of the glass surface. This allows selective monitoring of the subsarcolemmal region with TIRF, *versus* the entire cell with epifluorescence (Fig. 4*a*) (or ~ 500 nm depth with confocal microscopy). PDBu, ET1, and PE all induced significant membrane recruitment (121 ± 15 , 42 ± 4 , and $5 \pm 1\%$, respectively) (Fig. 4*b*, supplemental Fig. S1, and supplemental Movie S1), consistent in order of potency with the confocal results (Fig. 3*b*). Although the amount of PKD1 recruitment to the membrane with PE is only 4–12% of that induced by ET1, the initial rate of recruitment is similar (Fig. 4*c*), but it peaks earlier with PE ($t_{1/2} = 33$ *versus* 78 s) and partly declines by 100–200 s (Fig. 4*d*). This is consistent with transient residence of PKD1 at the SL with PE, with subsequent rapid translocation to the nucleus. The TIRF-measured membrane recruitment is transient if the stimulus is removed (not shown).

Fluorescence recovery after photobleach (FRAP) in TIRF mode provides additional local information about the degree of PKD1 membrane association: slow recovery indicates stably membrane-bound PKD, whereas fast recovery indicates more mobile PKD. Fig. 5*a* shows activation with agonist to steady state, followed by spot photobleach (see bleach spot in Fig. 5*c*

Divergence of PKD Activation

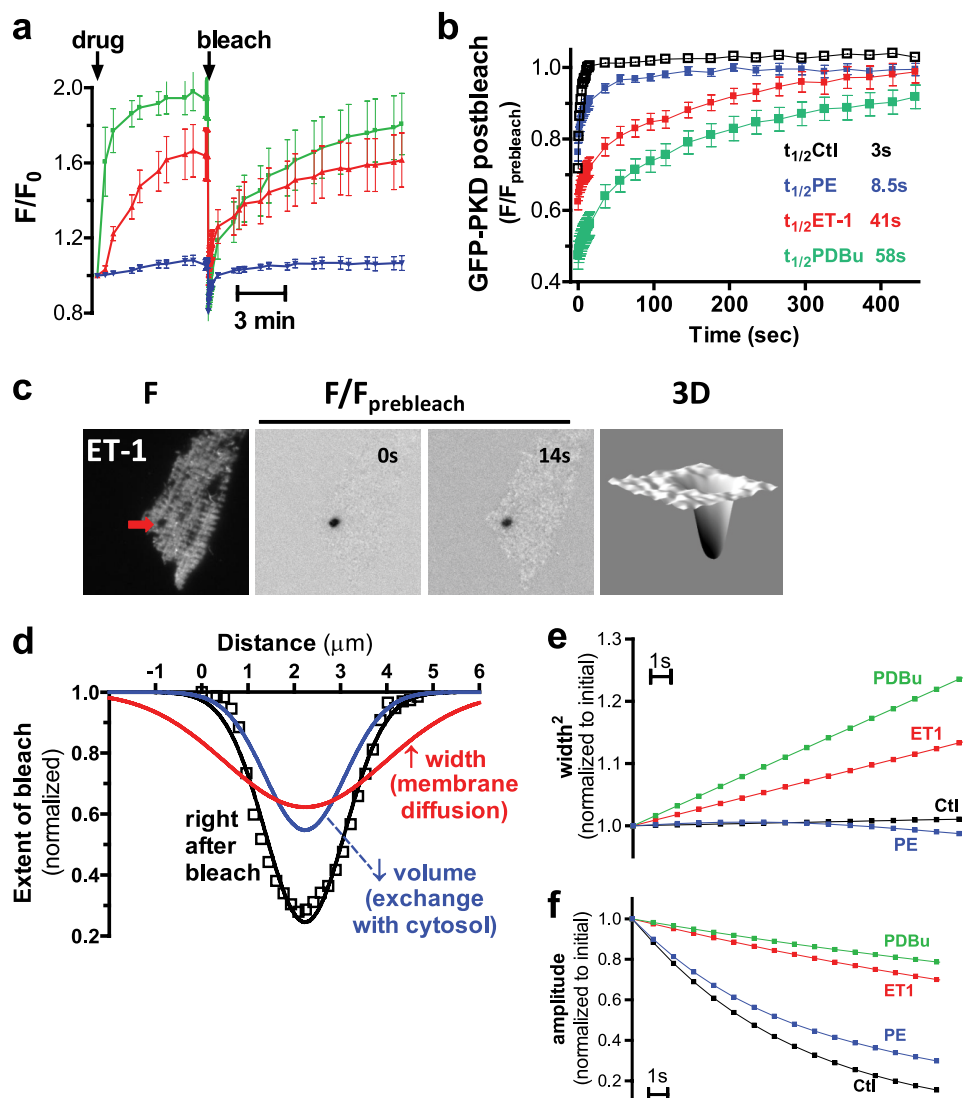


FIGURE 5. FRAP analysis of PKD membrane association. *a*, fluorescence recovery after spot photobleaching in TIRF mode. Target site was bleached after steady-state was reached for agonist-dependent membrane recruitment ($n = 8$). *b*, FRAP portion of signals in *a*, normalized to steady state recovery ($t_{1/2}$ for PE significantly different versus Ctl and also versus ET and PDBu). *c*, selective ablation of fluorescence at the target site (red arrow or dark spot in ratio image) is shown in TIRF images at the left and middle. Right panel is a three-dimensional isosurface rendering of the bleach spot. *d*, spatial profile of bleach spot, which is plotted as fluorescence versus distance across target site (squares, data points; lines, Gaussian fit/simulation). Recovery due to membrane (lateral) diffusion is seen as change in width, whereas recovery from the cytosol (PKD turnover) is seen as a change in volume. *e*, extraction of the width component of FRAP recovery (indicative of lateral membrane diffusion) and *f*, of the volume component (indicative of exchange with cytosol).

and supplemental Movie S2). The $t_{1/2}$ of FRAP in control, untreated myocytes was 3 s (Fig. 5*b*), indicating relatively free PKD1-GFP movement. After PDBu or ET1 treatment, the FRAP $t_{1/2}$ was greatly slowed (41–58 s), indicative of high specific binding of PKD1-GFP, and reduced mobility. After PE treatment, PKD1-GFP was only moderately slower than control ($t_{1/2} = 8.5$ s), suggesting relatively weak interactions of PKD1 at the membrane under these conditions, and relative high mobility. Thus, PE causes very rapid recruitment of PKD1 to the membrane, but also rapid release from the membrane, and this would explain the more rapid appearance of PKD1 in the nucleus upon PE activation (Fig. 3*b*). With ET1 (and PDBu) activation, PKD1 appears to come to the SL more slowly, but bind there more stably (explaining why little shows up in the nucleus, especially at short times).

We further analyzed the spatiotemporal profile of FRAP, where the bleached spot (red arrow) is normalized to the pre-

bleach intensity (Fig. 5*c*), allowing a three-dimensional surface plot of the bell-shape bleach profile, which is monitored during FRAP. Fig. 5*d* shows how the Gaussian profile would evolve by the process of diffusion along the membrane (change in width) or exchange with the cytosol (change in volume). Typical experiments are shown in Fig. 5, *e–f*. FRAP for PE seemed almost entirely due to a gain from the cytosol (pure reduction in amplitude/volume) and very little diffusion along the membrane (little increase in width). In contrast, FRAP for ET1 and PDBu appeared to be primarily due to membrane diffusion (increased width) with less exchange with the cytosol (smaller changes in volume). These findings confirm that PKD1 remains more mobile in response to PE (e.g. allowing release from the membrane and transit to the nucleus) than to ET1 or phorbol esters (Fig. 7). This may help to explain why HDAC5 nuclear export is so dominantly PKD/PKC dependent for PE, and less PKD dependent for ET1.

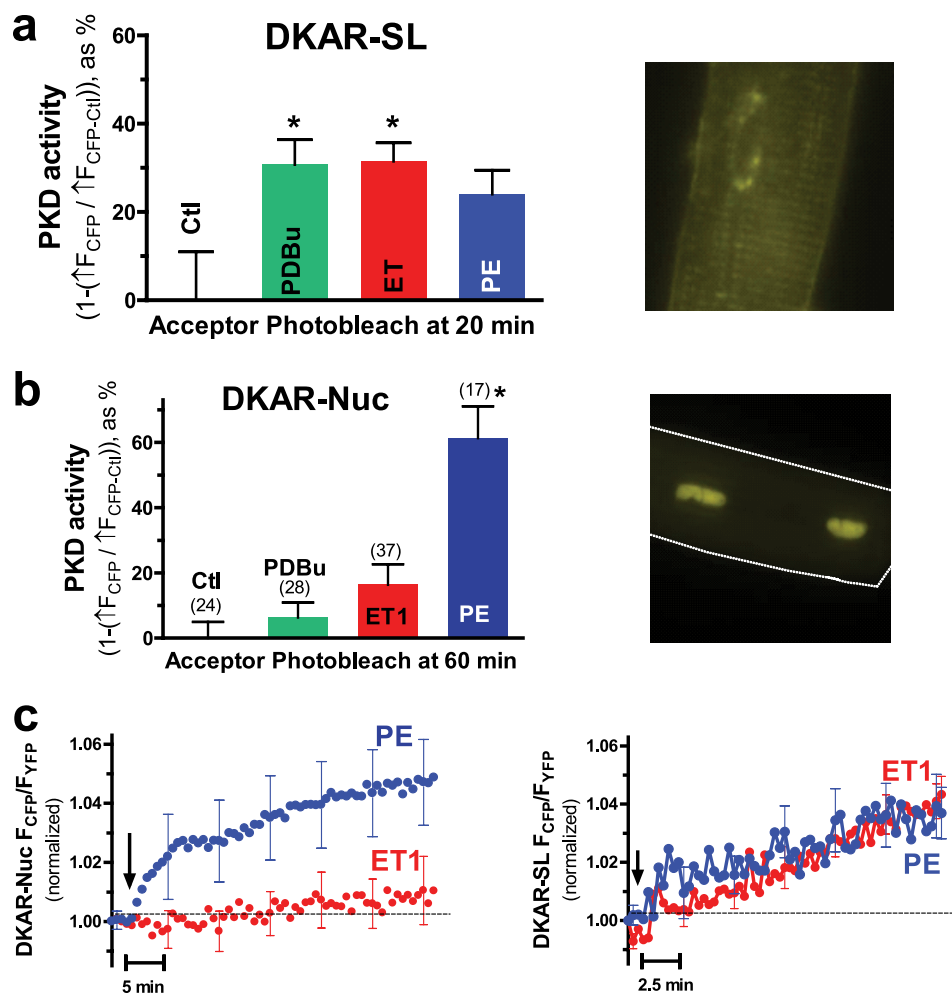


FIGURE 6. **Agonist-dependent activation of nuclear and sarcolemmal PKD activity.** *a*, PKD activity measured with sarcolemmal-targeted DKAR-SL. *Left*, acceptor photobleach-induced enhancement of donor fluorescence (FRET after 20 min agonist treatment, $n = 8$). *Right*, rabbit myocyte DKAR-SL localization. *b*, PKD activity measured with nuclear-targeted DKAR-Nuc. *Left*, acceptor photobleach measurement of FRET after 60 min agonist. *Right*, rabbit myocyte DKAR-Nuc localization. *c*, ratiometric, real time measurement of nuclear or membrane PKD activity (arrow indicates drug addition) ($n = 6$, PE curve and ET1 curve differ significantly for DKAR-Nuc, but not for DKAR-SL). *, $p < 0.05$ versus control.

Spatiotemporal Dynamics of PKD1 Activity in Response to PE and ET—We also targeted PKD activity reporters to the membrane and the nucleus: DKAR-SL and DKAR-Nuc, respectively. All 3 agonists elicited a similar increase in PKD activity at the SL (FRET was reduced 31 ± 5 , 31 ± 4 , and $24 \pm 5\%$ for PDBu, ET1 and PE, respectively; based on acceptor bleach induced donor enhancement) (Fig. 6*a*). In contrast, PE was much more potent in activating nuclear PKD than either ET1 or PDBu (Fig. 6*b*). This was also apparent in the real-time, ratiometric FRET measurements of nuclear and sarcolemmal PKD activity. PE and ET1 triggered similar responses at the sarcolemma, whereas ET1 caused a small, slow rise in nuclear PKD activity, whereas PE elicited a faster and larger response (Fig. 6*c*). These findings are consistent with a more pronounced nuclear role for PKD1 upon PE than ET1 stimulation.

DISCUSSION

PKD and CaMKII are critical signaling pathways that drive cardiac hypertrophy and pathological cardiac remodeling and are attractive drug targets (2, 5, 6). However, spatiotemporal features and detailed mechanisms of key neurohumoral regu-

lators (e.g. ET1 and PE) are unresolved. Here we show for the first time that the two G_q -coupled receptors ET1 and PE have highly distinct pathways that diverge in spatiotemporal activation of PKD and CaMKII, but converge in activation of HDAC5 nuclear export and transcriptional regulation. These parallel pathways may afford both signaling redundancy and unique cross-modulation between ET1 and PE and other signaling cascades that may differentially modulate one or the other pathway.

Role of PKD and CaMKII in HDAC5 Export—Both PKD and CaMKII are cardiac HDAC kinases, but Olson's group (4, 7) has suggested that HDAC5 phosphorylation is mediated by PKD, whereas HDAC4 is mediated by CaMKII (and HDAC4 has a CaMKII anchoring site). This was based on extensive HDAC studies in cell lines and cultured neonatal rat ventricular myocytes (and our neonatal myocyte data agrees with that).⁴ However, PKD is dramatically down-regulated in adult *versus* neonatal myocytes (38), such that the predominance of PKD on

⁴ K. Helmstadter, J. Bossuyt, J. L. Martin, and D. M. Bers, unpublished data.

Divergence of PKD Activation

HDAC5 translocation in adult ventricular myocytes may be less complete. Indeed, we showed that in adult ventricular myocytes ET1-induced HDAC5 nuclear export was dependent on local nuclear envelope InsP_3 -induced calcium release, and calmodulin was totally PKC-independent and that PKD and CaMKII contributed equally (37). Here we find that PE (another G_q -coupled hypertrophic agonist), induces a similar degree and rate of HDAC5 export and global PKD activation, but uses a very different signaling cascade. PE-induced HDAC5 phosphorylation and export is entirely PKC- and PKD-dependent, but entirely independent of InsP_3 or CaMKII activation. The latter pathway is consistent with observations in neonatal myocytes, but raises new questions about how ET1 and PE pathways diverge, and then converge via differential nuclear CaMKII and PKD activation at the HDAC5 level.

Role of InsP_3 in HDAC5 Export—Many G protein-coupled receptors activate phospholipases to produce both InsP_3 and DAG, the latter of which activates several PKC isoforms. Activated PKCs then cause many downstream effects (including PKD activation), some of which alter transcription. We developed (45) a fluorescent InsP_3 sensor and showed that ET1 and PE both induced rapid and similar increases in $[\text{InsP}_3]$ in adult cat ventricular myocytes, and that InsP_3 readily diffuses to the nucleus. This raises the question, why PE-induced HDAC5 export fails to occur when PKC is blocked? It is possible that the respective G_q -coupled receptors for PE and ET1 are at distinct locations within the adult cardiomyocyte, resulting in distinct $[\text{InsP}_3]$ patterns (e.g. with the InsP_3 signal not reaching the nucleus for PE). Alternatively, there could be differences in the balance of $[\text{InsP}_3]/[\text{DAG}]$ produced or how InsP_3 or DAG couple to PKD or CaMKII activation. Here we focused on spatiotemporal aspects of PKD activation.

Global Versus Local Spatiotemporal PKD Activity and Localization—Both ET1 and PE produced comparable global PKD activation in adult rabbit myocytes, based on global PKD-916 phosphorylation and FRET-based activity measurements with DKAR. However, a clue to differential activation pathways was that ET1 induced weaker PKD phosphorylation at PKC target sites ($\text{Ser}^{744}/\text{Ser}^{748}$), despite comparable phosphorylation at the putative autophosphorylation site (Ser^{916}). That is, ET1 might activate PKD without PKC activity, and this is consistent with our observation that ET1-induced HDAC5 nuclear export is partially PKD-dependent, but insensitive to PKC inhibition. This PKC independence of PKD activation (insensitivity to BisI inhibition) was also observed in neonatal rat ventricular myocytes (8) although this was not reflected in decreased phosphorylation levels at the PKC target sites. Moreover in neonatal rat ventricular myocytes the nuclear import of PKD for both agonists was similar. Our spatiotemporal analysis of PKD localization and activation in adult myocytes helped to clarify this pathway difference in the cell type where hypertrophic signaling is of interest for cardiac disease.

The canonical PKD activation pathway (although others have been suggested) involves phospholipase-generated DAG, which acts in 2 ways: (i) recruits cytosolic PKD to the membrane and (ii) recruits and activates PKC isoforms at the membrane, where novel PKCs then activate PKD by phosphorylation of the activation loop ($\text{Ser}^{744}/\text{Ser}^{748}$) (46, 47). In adult

cardiomyocytes we show that PKD1 rapidly translocates to the sarcolemma upon ET1 and PE exposure. Indeed, during the first 10–20 s the absolute rate of PKD1 appearance at the membrane was comparable for ET1 and PE (Fig. 4c), but the rapid nuclear translocation of PKD upon PE-induced activation caused the peak membrane (PKD) to occur earlier in time and be smaller in amplitude compared with ET1 activation. This is consistent with the notion that PKD phosphorylation at $\text{Ser}^{744}/\text{Ser}^{748}$ facilitates release of PKD from the membrane and translocation to intracellular targets (e.g. nucleus, Golgi...) (46). Our results also suggest that ET1 can activate PKD at the sarcolemma without PKC-dependent phosphorylation, and in this case PKD remains membrane associated (perhaps because of binding to different molecular partners where it could phosphorylate other membrane targets). Thus, our fluorescence measurements (confocal, TIRF, and FRAP) show that the spatiotemporal dynamics of PKD translocation are stimulus-specific with a more rapid nuclear translocation of activated PKD upon PE activation. Recently, the O'Connell group (48) suggested that α -adrenergic receptors are largely perinuclear. If this is correct, an alternative interpretation to our findings is that the lower sarcolemmal PKD1 recruitment observed with TIRF and confocal imaging was because the PE activation effect was occurring mainly at the nuclear membrane (rather than faster sarcolemmal to nuclear translocation). However, our confocal data do not show appreciable perinuclear membrane recruitment in response to PE. Also, the initial PE-induced PKD1 recruitment to the sarcolemma (Fig. 4c) and similar activity signal with DKAR (Fig. 6c) seem somewhat more consistent with a major part of the PE-induced effect initiating at the sarcolemma. The data also help to explain why HDAC5 phosphorylation and translocation is so strongly PKD-dependent for PE versus ET1. However, we cannot exclude that some portion of the PE-induced nuclear PKD activation is occurring near internal α -adrenergic receptors.

The very slow and smaller amplitude ET1-induced PKD nuclear translocation and activity (Figs. 3 and 6) may allow InsP_3 - and CaMKII-dependent HDAC5 to occur (where PKD and CaMKII contribute equally to HDAC5 nuclear export) (37). Although these results add satisfying mechanistic detail with respect to how different strengths of nuclear PKD activation occur for PE and ET1 activation, three questions will require further study. First, what are the molecular interactions at the membrane that dictate rapid PKD nuclear translocation (for PE) and retention at the sarcolemma (for ET1)? Second, how is PKD activated by PKC-independent mechanisms in response to ET1 (in contrast to PE)? PKC-independent mechanisms of PKD activation have been described (31, 32, 47), but are generally slower than what we report here. Third, what prevents the PE-induced InsP_3 from activating CaMKII-dependent HDAC5 phosphorylation (as seen for ET1 activation) when PKC is inhibited? It is possible that InsP_3 produced during PE activation is degraded prior to reaching the nuclear InsP_3 -CaMKII complex or that PE activates a parallel pathway diminishing the InsP_3 responsiveness. The differential spatiotemporal signaling at the endothelin and α -adrenergic receptor that we have uncovered should pave the way to understanding critical new aspects of local receptor complex function.

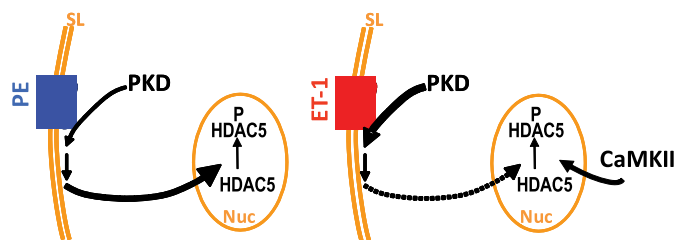


FIGURE 7. **Working hypothesis of PKD activation.** PE shifts PKD to the sarcolemma where it is activated and rapidly translocates to the nucleus (rapid membrane-cytosolic movement). ET1 (like PDBu) causes sarcolemmal PKD recruitment and activation, but PKD remains largely membrane bound, with only slow and small nuclear translocation.

Local Versus Global PKD Activity—Sarcolemmal-targeted DKAR failed to detect differences in sarcolemmal-localized PKD activity with PE, ET1, or PDBu. The relatively strong signals there (25–30% reduction in FRET (Fig. 6a)) would be consistent with nearly maximal PKD activity at the sarcolemma with all three agonists. If that is true, it would indicate that even the relatively small amount of PKD1 recruited to the sarcolemma by PE (*versus* ET1 or PDBu (Figs. 2b and 4b)) is sufficient to fully phosphorylate DKAR localized at the membrane. Then, the higher sarcolemmal PKD accumulation with ET1 would have enhanced capacity to phosphorylate additional sarcolemmal targets, which may have lower PKD affinity than DKAR.

Nuclear PKD recruitment and activity is faster and larger for PE *versus* ET1 (Figs. 3b and 6, b and c). However, even the moderate levels of nuclear PKD achieved with ET1 are sufficient for partial PKD-dependent HDAC5 phosphorylation and nuclear export when CaMKII is inhibited (Fig. 1d and Ref. 37). Although this may mean that a small amount of nuclear PKD is sufficient to trigger substantial HDAC5 nuclear export, PKD may also function in the cytosol to re-phosphorylate HDAC5 that is dephosphorylated there, keeping HDAC5 more cytosolic (as shown for CaMKII δ) (49). Nevertheless, the faster and larger rise of PKD activity in the nucleus for PE *versus* ET1 (Fig. 6c) is entirely consistent with a more prominent nuclear role for PKD1 upon PE stimulation (*versus* ET1) and with a critical role in the regulation of HDAC5. The present study highlights how precise control of spatial and temporal dynamics of PKD1 activity and localization direct the cell responses in a stimulus-specific manner. This may be the key to developing effective therapeutic approaches to reverse pathological remodeling and improve cardiac dysfunction.

In summary, the data here reveal highly distinct spatiotemporal patterns of PKD activation and translocation in adult ventricular myocytes in response to the activation of endothelin or α -adrenergic receptors by ET1 and PE. PE and ET1 drive rapid sarcolemmal recruitment and activation of PKD, but with PE activation PKD then is rapidly shuttled to the nucleus where PKD can activate HDAC5 nuclear export (Fig. 7). In contrast, after ET1 activation PKD is much more stably bound at the membrane, with only slower and smaller nuclear translocation (and nuclear HDAC5 export). The experiments highlight how spatiotemporal dynamics of PKD1 constitute an elegant fine tuning system that controls the cell response and location-specific interactions with other signaling pathways. This reinforces the idea that PKD inhibition may be beneficial therapeutically

by keeping this HDAC5-dependent hypertrophic pathway in check. However, it also demonstrates that α -adrenergic and ET1 receptor activation follow distinct spatiotemporal pathways that may afford unique interactions with other cellular signaling pathways.

Acknowledgments—We thank Linda Lee for help with the adenoviral work and immunocytochemistry and Khanhha Dao for myocyte preparation.

REFERENCES

1. Frey, N., and Olson, E. N. (2003) *Annu. Rev. Physiol.* **65**, 45–79
2. McKinsey, T. A. (2007) *Cardiovasc. Res.* **73**, 667–677
3. Avkiran, M., Rowland, A. J., Cuello, F., and Haworth, R. S. (2008) *Circ. Res.* **102**, 157–163
4. Backs, J., Backs, T., Bezprozvannaya, S., McKinsey, T. A., and Olson, E. N. (2008) *Mol. Cell. Biol.* **28**, 3437–3445
5. Fielitz, J., Kim, M. S., Shelton, J. M., Qi, X., Hill, J. A., Richardson, J. A., Bassel-Duby, R., and Olson, E. N. (2008) *Proc. Natl. Acad. Sci. U.S.A.* **105**, 3059–3063
6. Backs, J., Backs, T., Neef, S., Kreuzer, M. M., Lehmann, L. H., Patrick, D. M., Grueter, C. E., Qi, X., Richardson, J. A., Hill, J. A., Katus, H. A., Bassel-Duby, R., Maier, L. S., and Olson, E. N. (2009) *Proc. Natl. Acad. Sci. U.S.A.* **106**, 2342–2347
7. Vega, R. B., Harrison, B. C., Meadows, E., Roberts, C. R., Papst, P. J., Olson, E. N., and McKinsey, T. A. (2004) *Mol. Cell. Biol.* **24**, 8374–8385
8. Harrison, B. C., Kim, M. S., van Rooij, E., Plato, C. F., Papst, P. J., Vega, R. B., McAnally, J. A., Richardson, J. A., Bassel-Duby, R., Olson, E. N., and McKinsey, T. A. (2006) *Mol. Cell. Biol.* **26**, 3875–3888
9. Zhang, T., Maier, L. S., Dalton, N. D., Miyamoto, S., Ross, J., Jr., Bers, D. M., and Brown, J. H. (2003) *Circ. Res.* **92**, 912–919
10. Bossuyt, J., Helmstadter, K., Wu, X., Clements-Jewery, H., Haworth, R. S., Avkiran, M., Martin, J. L., Pogwizd, S. M., and Bers, D. M. (2008) *Circ. Res.* **102**, 695–702
11. Ghanekar, Y., and Lowe, M. (2005) *Trends Cell Biol.* **15**, 511–514
12. Jaggi, M., Du, C., Zhang, W., and Balaji, K. C. (2007) *Front. Biosci.* **12**, 3757–3767
13. Trauzold, A., Schmiedel, S., Sipos, B., Wermann, H., Westphal, S., Röder, C., Klapper, W., Arlt, A., Lehnert, L., Ungefroren, H., Johannes, F. J., and Kalthoff, H. (2003) *Oncogene* **22**, 8939–8947
14. Maier, L. S., and Bers, D. M. (2007) *Cardiovasc. Res.* **73**, 631–640
15. Chang, S., McKinsey, T. A., Zhang, C. L., Richardson, J. A., Hill, J. A., and Olson, E. N. (2004) *Mol. Cell. Biol.* **24**, 8467–8476
16. Zhang, C. L., McKinsey, T. A., Chang, S., Antos, C. L., Hill, J. A., and Olson, E. N. (2002) *Cell* **110**, 479–488
17. Lavalle, C. R., George, K. M., Sharlow, E. R., Lazo, J. S., Wipf, P., and Wang, Q. J. (2010) *Biochim. Biophys. Acta* **1806**, 183–192
18. Liu, F., Levin, M. D., Petrenko, N. B., Lu, M. M., Wang, T., Yuan, L. J., Stout, A. L., Epstein, J. A., and Patel, V. V. (2008) *J. Mol. Cell. Cardiol.* **45**, 715–723
19. Cho, Y. K., Eom, G. H., Kee, H. J., Kim, H. S., Choi, W. Y., Nam, K. I., Ma, J. S., and Kook, H. (2010) *Circ. J.* **74**, 760–770
20. Stimson, L., Wood, V., Khan, O., Fotheringham, S., and La Thangue, N. B. (2009) *Ann. Oncol.* **20**, 1293–1302
21. Beumer, J. H., and Tawbi, H. (2010) *Curr. Clin. Pharmacol.* **5**, 196–208
22. Ling, H., Zhang, T., Pereira, L., Means, C. K., Cheng, H., Gu, Y., Dalton, N. D., Peterson, K. L., Chen, J., Bers, D., and Heller Brown, J. (2009) *J. Clin. Invest.* **119**, 1230–1240
23. Monovich, L., Vega, R. B., Meredith, E., Miranda, K., Rao, C., Capparelli, M., Lemon, D. D., Phan, D., Koch, K. A., Chapo, J. A., Hood, D. B., and McKinsey, T. A. (2010) *FEBS Lett.* **584**, 631–637
24. Meredith, E. L., Ardayfio, O., Beattie, K., Dobler, M. R., Enyed, I., Gaul, C., Hosagrahara, V., Jewell, C., Koch, K., Lee, W., Lehmann, H., McKinsey, T. A., Miranda, K., Pagratis, N., Pancost, M., Patnaik, A., Phan, D., Plato, C., Qian, M., Rajaraman, V., Rao, C., Rozhitskaya, O., Ruppen, T., Shi, J.,

Divergence of PKD Activation

- Siska, S. J., Springer, C., van Eis, M., Vega, R. B., von Matt, A., Yang, L., Yoon, T., Zhang, J. H., Zhu, N., and Monovich, L. G. (2010) *J. Med. Chem.* **53**, 5400–5421
25. Meredith, E. L., Beattie, K., Burgis, R., Capparelli, M., Chapo, J., Dipietro, L., Gamber, G., Enyedy, I., Hood, D. B., Hosagrahara, V., Jewell, C., Koch, K. A., Lee, W., Lemon, D. D., McKinsey, T. A., Miranda, K., Pagratis, N., Phan, D., Plato, C., Rao, C., Rozhitskaya, O., Soldermann, N., Springer, C., van Eis, M., Vega, R. B., Yan, W., Zhu, Q., and Monovich, L. G. (2010) *J. Med. Chem.* **53**, 5422–5438
26. Harikumar, K. B., Kunnumakkara, A. B., Ochi, N., Tong, Z., Deorukhkar, A., Sung, B., Kelland, L., Jamieson, S., Sutherland, R., Raynham, T., Charles, M., Bagherzadeh, A., Bagherzadeh, A., Foxton, C., Boakes, A., Farooq, M., Maru, D., Diagaradjane, P., Matsuo, Y., Sinnett-Smith, J., Gelovani, J., Krishnan, S., Aggarwal, B. B., Rozengurt, E., Ireson, C. R., and Guha, S. (2010) *Mol. Cancer Ther.* **9**, 1136–1146
27. Valverde, A. M., Sinnett-Smith, J., Van Lint, J., and Rozengurt, E. (1994) *Proc. Natl. Acad. Sci. U.S.A.* **91**, 8572–8576
28. Sturany, S., Van Lint, J., Muller, F., Wilda, M., Hameister, H., Hocker, M., Brey, A., Gern, U., Vandenheede, J., Gress, T., Adler, G., and Seufferlein, T. (2001) *J. Biol. Chem.* **276**, 3310–3318
29. Hayashi, A., Seki, N., Hattori, A., Kozuma, S., and Saito, T. (1999) *Biochim. Biophys. Acta* **1450**, 99–106
30. Newton, A. C., and Johnson, J. E. (1998) *Biochim. Biophys. Acta* **1376**, 155–172
31. Wang, Q. J. (2006) *Trends Pharmacol. Sci.* **27**, 317–323
32. Rozengurt, E., Rey, O., and Waldron, R. T. (2005) *J. Biol. Chem.* **280**, 13205–13208
33. Rey, O., Reeve, J. R., Jr., Zhukova, E., Sinnett-Smith, J., and Rozengurt, E. (2004) *J. Biol. Chem.* **279**, 34361–34372
34. Waldron, R. T., and Rozengurt, E. (2003) *J. Biol. Chem.* **278**, 154–163
35. Matthews, S. A., Rozengurt, E., and Cantrell, D. (1999) *J. Biol. Chem.* **274**, 26543–26549
36. Kunkel, M. T., Toker, A., Tsien, R. Y., and Newton, A. C. (2007) *J. Biol. Chem.* **282**, 6733–6742
37. Wu, X., Zhang, T., Bossuyt, J., Li, X., McKinsey, T. A., Dedman, J. R., Olson, E. N., Chen, J., Brown, J. H., and Bers, D. M. (2006) *J. Clin. Invest.* **116**, 675–682
38. Haworth, R. S., Goss, M. W., Rozengurt, E., and Avkiran, M. (2000) *J. Mol. Cell Cardiol.* **32**, 1013–1023
39. Bassani, J. W., Bassani, R. A., and Bers, D. M. (1994) *J. Physiol.* **476**, 279–293
40. Van Munster, E. B., Kremers, G. J., Adjobo-Hermans, M. J., and Gadella, T. W., Jr. (2005) *J. Microsc.* **218**, 253–262
41. Kelly, E. M., Hou, Z., Bossuyt, J., Bers, D. M., and Robia, S. L. (2008) *J. Biol. Chem.* **283**, 12202–12211
42. Robia, S. L., Campbell, K. S., Kelly, E. M., Hou, Z., Winters, D. L., and Thomas, D. D. (2007) *Circ. Res.* **101**, 1123–1129
43. Rey, O., Sinnett-Smith, J., Zhukova, E., and Rozengurt, E. (2001) *J. Biol. Chem.* **276**, 49228–49235
44. Matthews, S. A., Iglesias, T., Rozengurt, E., and Cantrell, D. (2000) *EMBO J.* **19**, 2935–2945
45. Remus, T. P., Zima, A. V., Bossuyt, J., Bare, D. J., Martin, J. L., Blatter, L. A., Bers, D. M., and Mignery, G. A. (2006) *J. Biol. Chem.* **281**, 608–616
46. Rykx, A., De Kimpe, L., Mikhalap, S., Vantus, T., Seufferlein, T., Vandenheede, J. R., and Van Lint, J. (2003) *FEBS Lett.* **546**, 81–86
47. Jacamo, R., Sinnett-Smith, J., Rey, O., Waldron, R. T., and Rozengurt, E. (2008) *J. Biol. Chem.* **283**, 12877–12887
48. Wright, C. D., Chen, Q., Baye, N. L., Huang, Y., Healy, C. L., Kasinathan, S., and O'Connell, T. D. (2008) *Circ. Res.* **103**, 992–1000
49. Zhang, T., Kohlhaas, M., Backs, J., Mishra, S., Phillips, W., Dybkova, N., Chang, S., Ling, H., Bers, D. M., Maier, L. S., Olson, E. N., and Brown, J. H. (2007) *J. Biol. Chem.* **282**, 35078–35087